Infrared- and Raman-active modes of Bi-based cuprate superconductors calculated in a microscopic model

2003 J. Phys.: Condens. Matter 15 8495

(http://iopscience.iop.org/0953-8984/15/49/024)

INSTITUTE OF PHYSICS PUBLISHING JOURNAL OF PHYSICS: CONDENSED MATTER

J. Phys.: Condens. Matter **15** (2003) 8495–8511 PII: S0953-8984(03)68136-1

Infrared- and Raman-active modes of Bi-based cuprate superconductors calculated in a microscopic model

Claus Falter and Frank Schnetgöke

Institut für Festkörpertheorie, Universität Münster, Wilhelm-Klemm-Straße 10, 48149 Münster, Germany

E-mail: Falter@nwz.uni-muenster.de

Received 29 August 2003
Published 25 November 2003
Online at stacks.iop.org/JPhysCM/15/8495

Abstract

We present phonon frequencies and eigenvectors for the *c*-axis-polarized infrared- and Raman-active modes of A_{2u} and A_{1g} symmetry in the single-layer $Bi_2Sr_2CuO_6$ (Bi-2201) and the bilayer $Bi_2Sr_2CaCu_2O_8$ (Bi-2212) cuprate superconductors within our recently proposed microscopic formulation of the electronic density response and lattice dynamics in high-temperature superconductors (HTSCs). The model includes localized electronic charge-fluctuations as well as anisotropic dipole-fluctuations. The former have been shown to be the dominating polarization process in the CuO planes while the latter are particularly important for the ions in the ionic layers of the HTSC. The effect of both types of screening contribution on the *c*-axis lattice dynamics of the Bi-based cuprates is investigated. A characteristic and strong renormalization of certain A_{2u} and A_{1g} modes is shown to be related to the metallicity of the BiO layers. We obtain a good agreement between the calculated A_{2u} frequencies and new experimental results obtained by ellipsometric measurements on single crystals and propose an assignment of the modes. Moreover, the calculated A_{1g} Raman modes and eigenvectors are compared with measured frequencies and the contradictory assignments of the modes found in the literature.

1. Introduction

High-temperature superconductors (HTSCs) are characterized by an anisotropic mixed ionic–covalent–metallic bonding behaviour. The ionic nature of these materials dominates along the *c*-axis mostly in the ionic layers. On the other hand, specific covalent–metallic bonding contributions become important in the CuO plane. In contrast to conventional metals and superconductors, these specific bonding contributions are not well described within the

homogenous electron-gas picture because most of the electronic charge is concentrated at the ions constituting the crystal, and thus a localized ionic description of the density response and screening is appropriate.

Our microscopic modelling of screening and lattice dynamics of the HTSC in the framework of the linear response approach focuses just on these specific electronic features of the cuprate superconductors. The ionic nature of the HTSC is described by an *ab initio* rigid-ion model (RIM) leading to a local rigid charge response and electron–phonon interaction (EPI), while the nonlocal, nonrigid part of the electronic density response is modelled by microscopically well defined charge- and dipole-fluctuations (CFs and DFs), respectively. From a general point of view our treatment of the density response, EPI and lattice dynamics can be considered as a microscopic (semi-*ab initio*) implementation of a combination of the well known phenomenological dipole shell model and a charge fluctuation model, respectively. For a general discussion of phenomenological models of lattice dynamics that use localized electronic variables as adiabatic degrees of freedom, see for example [1]. While in this approach the coupling coefficients enter the calculations as fitting parameters, which are not unique, and so the real bonding structure of the crystal might be not accounted for properly, the essential aspect of our microscopic model is that it allows for a calculation of all the couplings appearing in the dynamical matrix and the EPI. For example, the covalent metallic features of bonding in the HTSC are taken approximately into account by the electronic bandstructure: first, in a global way by using (static) effective ionic charges in the RIM (ion softening), as calculated from a tight-binding analysis of the (first-principles) electronic bandstructure, and second, via the electronic polarizability, which contains the kinetic one-particle part of the charge response; see section 2.

There has been a great deal of interest in the electron–phonon coupling of the HTSCs after the discovery of strong coupling to a mode at about 70 meV in a large number of cuprates [2]. The coupling was ascribed to high-frequency copper–oxygen bond-stretching modes predicted previously as strong-coupling modes by our calculations of the phonon dispersion of La_2CuO_4 and $YBa_2Cu_3O_7$ within the microscopic model outlined in section 2 and also used for the Bi-based cuprates in this paper [3–6]. These calculations have revealed the type of charge response leading to a large EPI and an anomalous strong softening of the modes, also seen in the experiments [7–9] when the cuprates are doped. Nonlocal EPI effects of ionic charge fluctuation type have been shown in [3–6] to be the microscopic reason for these coupling effects. Moreover, using La_2CuO_4 as an example [10, 11], we have applied our model to investigate *c*-axis phonons and the *c*-axis charge response in the HTSC, which is a subject of controversial discussion and is still not well understood. In the present paper we extend our investigations of the *c*-axis lattice dynamics of the Bi-based cuprates and calculate the *c*-axis-polarized infrared- (IR-) and Raman-active modes for the single-layer $Bi_2Sr_2CuO_6$ (Bi-2201) and the bilayer $Bi_2Sr_2CaCu_2O_8$ (Bi-2212) superconductors. The assignments of the *c*-axis A_{2u}-IR-phonons are discussed controversially in the literature [12, 13]. Theoretical calculations of Raman- and infrared-active modes have been presented so far using the empirical shell model [14, 15] and a force constant model [16], respectively. As far as the Raman-active A_{1g} modes are concerned different experimental groups have published rather different and contradictory assignments [17–19], see e.g. the tabulated frequencies and different assignments listed in [17] for Bi-2212. In particular the origin of the high-frequency vibrations around 460 and 630 cm^{-1} in the Raman spectra of Bi-2212 is controversial and there is a strong dispute among the different experimental groups concerning the question of which mode can be attributed to the oxygens O2 located in the SrO plane and which one to the oxygens O3 in the BiO plane. Our results concerning this question clearly assign the 630 cm^{-1} phonon to the vibrations of the apical oxygen ions O2 located in the SrO layers.

In order to provide a certain degree of self-consistency of the paper, in section 2 a résumé of the theory and modelling is given. Section 3 deals with the calculations and the discussion. Specific model considerations and structural aspects are considered. Then the results for the A_{2u} and A_{1g} phonon frequencies and the corresponding displacement patterns for Bi-2201 and Bi-2212 are shown. A comparison with the available theoretical calculations and the experimental data is presented. Concerning the A_{2u} modes, new results as obtained from ellipsometry experiments on single crystals of high quality are used for the comparison [15]. Section 4 contains a summary and the conclusions.

2. Résumé of the theory and modelling

In this section we outline the theory and modelling of our microscopic approach of the electronic density response, the lattice dynamics and the EPI in the HTSC. A detailed description can be found [3, 20]. In this formulation the local part of the electronic charge response is approximated by an *ab initio* RIM taking into account ion softening in terms of (static) effective ionic charges as calculated from a tight-binding analysis of the electronic bandstructure. In addition, scaling of the short-range part of certain pair potentials between the ions is considered in order to simulate additional covalence effects in the calculations [21]. Scaling is performed in such a way that the energy-minimized structure is a close as possible to the experimental one. The tight-binding analysis supplies the effective ionic charges as extracted from the orbital occupation numbers Q_μ of the μ (tight-binding) orbital in question:

$$Q_\mu = \frac{2}{N} \sum_{n\vec{k}} |C_{\mu n}(\vec{k})|^2. \tag{1}$$

$C_{\mu n}(\vec{k})$ stands for the μ component of the eigenvector of band n at wavevector $\vec{k}$ in the first Brillouin zone; the summation in equation (1) runs over all occupied states and N gives the number of elementary cells in the (periodic) crystal. The RIM with the corrections just mentioned then serves as a reference system for the description of the HTSC. For a representation of the (nonrigid) electronic density response and screening in the HTSC, particularly in the metallic phase, more or less localized electronic CFs in the outer shells of the ions are considered. The latter dominate the long-ranged, nonlocal contribution of the electronic density response and the EPI in the HTSC. In addition, DFs are treated within our approach [20, 22]. Thus, the starting point of our model is the ionic densities in the perturbed state which are given by

$$\rho_\alpha(\vec{r}) = \rho_\alpha^0(r) + \sum_\lambda Q_\lambda \rho_\lambda^{\mathrm{CF}}(r) + \vec{p}_\alpha \cdot \hat{r}\, \rho_\alpha^{\mathrm{D}}(r). \tag{2}$$

ρ_α^0 is the density of the unperturbed ion localized at the sublattice α of the crystal. The Q_λ and $\rho_\lambda^{\mathrm{CF}}$ describe the amplitudes and the form-factors of the CFs and the last term in equation (2) gives the dipolar deformation of an ion α with amplitude (dipole moment) $\vec{p}_\alpha$ and a radial density distribution ρ_α^{D}. $\hat{r}$ is the unit vector in the direction of $\vec{r}$. The $\rho_\lambda^{\mathrm{CF}}$ are approximated by a spherical average of the orbital densities of the outer ionic shells calculated in the local-density approximation (LDA) taking self-interaction effects (SIC) into account. The dipole density ρ_α^{D} is obtained from a modified Sternheimer method in the framework of LDA-SIC [20].

The total energy of the crystal is investigated by assuming that the density of the crystal can be approximated by a superposition of overlapping densities of the individual ions, ρ_α. The ρ_α^0 are calculated within LDA-SIC taking environment effects, via a Watson sphere potential, and the calculated static effective charges of the ions into account. Such an approximation

holds well in the HTSC [21, 23]. Moreover, applying the pair-potential approximation we get for the total energy:

$$E(R,\zeta) = \sum_{\vec{a}\alpha} E_\alpha^{\vec{a}}(\zeta) + \tfrac{1}{2}{\sum_{\substack{\vec{a}\alpha \\ \vec{b}\beta}}}' \phi_{\alpha\beta}(\vec{R}_\beta^{\vec{b}} - \vec{R}_\alpha^{\vec{a}}, \zeta). \tag{3}$$

The energy E depends on the configuration of the ions $\{R\}$ and the electronic degrees of freedom (EDFs) $\{\zeta\}$ of the charge density, i.e. $\{Q_\lambda\}$ and $\{\vec{p}_\alpha\}$ in equation (2). $E_\alpha^{\vec{a}}$ are the energies of the single ions. $\vec{a}$ and $\vec{b}$ denote the elementary cells in the crystal and α and β the sublattices. The second term in equation (3) is the interaction energy of the system, expressed by the anisotropic pair-interactions $\phi_{\alpha\beta}$. The prime in equation (3) means that the self-term has to be omitted. Both $E_\alpha^{\vec{a}}$ and $\phi_{\alpha\beta}$ in general depend upon ζ via ρ_α.

From the adiabatic condition

$$\frac{\partial E(R,\zeta)}{\partial \zeta} = 0, \tag{4}$$

an expression for the force constants, and accordingly, the dynamical matrix in the harmonic approximation can be derived.

$$t_{ij}^{\alpha\beta}(\vec{q}) = [t_{ij}^{\alpha\beta}(\vec{q})]_{\mathrm{RIM}} - \frac{1}{\sqrt{M_\alpha M_\beta}} \sum_{\kappa,\kappa'} [B_i^{\kappa\alpha}(\vec{q})]^* [C^{-1}(\vec{q})]_{\kappa\kappa'} B_j^{\kappa'\beta}(\vec{q}). \tag{5}$$

$[t_{ij}^{\alpha\beta}(\vec{q})]_{\mathrm{RIM}}$ denotes the contribution of the RIM to the dynamical matrix. M_α and M_β are the masses of the ions and $\vec{q}$ is a wavevector from the first Brillouin zone.

The quantities $\vec{B}(\vec{q})$ and $C(\vec{q})$ in equation (5) represent the Fourier transforms of the coupling coefficients as calculated from the energy,

$$\vec{B}_{\kappa\beta}^{\vec{a}\vec{b}} = \frac{\partial^2 E(R,\zeta)}{\partial \zeta_\kappa^{\vec{a}}\, \partial \vec{R}_\beta^{\vec{b}}}, \tag{6}$$

and

$$C_{\kappa\kappa'}^{\vec{a}\vec{b}} = \frac{\partial^2 E(R,\zeta)}{\partial \zeta_\kappa^{\vec{a}}\, \partial \zeta_{\kappa'}^{\vec{b}}}. \tag{7}$$

The derivatives in equations (6) and (7) have to be performed at the equilibrium positions. κ denotes the EDF (CFs and DFs in the present model) in an elementary cell of the crystal. The $\vec{B}$ coefficients describe the coupling between the EDF and the ions, and the C coefficients the interaction between the EDFs.

The phonon frequencies $\omega_\sigma(\vec{q})$ and the eigenvectors $\vec{e}^{\alpha}(\vec{q}\sigma)$ of the modes $(\vec{q}\sigma)$ then are obtained from the secular equation for the dynamical matrix given in equation (5), i.e.

$$\sum_{\beta j} t_{ij}^{\alpha\beta}(\vec{q}) e_j^\beta(\vec{q}) = \omega^2(\vec{q}) e_i^\alpha(\vec{q}). \tag{8}$$

Equations (5)–(8) are generally valid and, in particular, are independent of our specific model for the decomposition of the perturbed density in equation (2) and of the pair approximation (3) for the energy.

The pair-interactions $\phi_{\alpha\beta}$ can be decomposed into long-ranged Coulomb contributions and short-ranged terms. The latter are separated into the interaction between the ion cores and the charge density from equation (2), the interaction between the density ρ_α with the density ρ_β (Hartree contribution) and a term representing the sum of the kinetic one-particle and the exchange–correlation contribution of the interaction between the two ions. A detailed description of the $\phi_{\alpha\beta}$ and the calculation of the coupling coefficients B and C for the EDF is

given in [20]. In this context it should be mentioned that the matrix $C_{\kappa\kappa'}(\vec{q})$ of the EDF–EDF interaction whose inverse appears in equation (5) for the dynamical matrix can be written as

$$C = \Pi^{-1} + \tilde{V}. \tag{9}$$

Π^{-1} contains the kinetic one-particle part to the interaction and $\tilde{V}$ the Hartree and exchange–correlation contribution. The quantity C^{-1} needed for the calculation of the dynamical matrix is closely related to the density response function (matrix) and to the inverse dielectric function (matrix) ε^{-1}, respectively. Written in matrix notation we have the relation

$$C^{-1} = \Pi(1 + \tilde{V}\Pi)^{-1} \equiv \Pi\varepsilon^{-1}, \qquad \varepsilon = 1 + \tilde{V}\Pi. \tag{10}$$

The CF–CF submatrix of the matrix Π can be calculated approximatively from a tight-binding analysis of the (first-principles) electronic bandstructure. In this case the electronic polarizability Π is given by

$$\Pi_{\kappa\kappa'}(\vec{q}) = -\frac{2}{N}\sum_{\substack{n,n'\\ \vec{k}}} \frac{f_{n'}(\vec{k}+\vec{q}) - f_n(\vec{k})}{E_{n'}(\vec{k}+\vec{q}) - E_n(\vec{k})}[C^*_{\kappa n}(\vec{k})C_{\kappa n'}(\vec{k}+\vec{q})][C^*_{\kappa' n}(\vec{k})C_{\kappa' n'}(\vec{k}+\vec{q})]^*. \tag{11}$$

f, E and C are the occupation numbers, the electronic bandstructure (single-particle energies) and the expansion coefficients of the Bloch-functions in terms of the tight-binding functions.

3. Calculations and discussion

3.1. Specific model considerations and structural data

If the incommensurate complex superstructures in the BiO plane as observed by diffraction experiments [24, 25] are neglected, the Bi-based cuprates are quite well represented by a body-centred-tetragonal structure with space group $I4/mmm$ [26, 27]. The elementary cells of $Bi_2Sr_2CuO_6$ (Bi-2201) and $Bi_2Sr_2CaCu_2O_8$ (Bi-2212) in the body-centred-tetragonal structure are displayed in figure 1. As a first approximation this structure has been used most frequently for the interpretation of the IR and Raman spectra. This is generally believed to provide a useful description of the most intense IR- and Raman-active phonon modes.

The origin of the superstructure is generally attributed to the mismatch between the BiO and CuO layers, and the weak coupling between the two BiO planes favours incommensurate distortions. The main difficulty in structural refinements then concerns the BiO layers. This may lead to complications in the interpretation of the phonon modes because the corresponding reduction of symmetry may lead in the actual measurement of the real materials to additional modes in the spectra.

According to first-principles calculations of the electronic structure [28, 29] the BiO layers contribute to bands of Bi p and O p character which dip below the Fermi energy in a small part of the Brillouin-zone (electron pockets). These bands may act as a metallic charge reservoir which provides electron pockets that allow for an increase in the number of holes in the CuO bands, promoting (super-)conductivity in the CuO layers. In the real material, however, the matter is far more complicated and it is currently not possible to account for the superstructure effects in first-principles calculations. The presence of the superstructure may also be a reason which greatly complicates the comparison with the experimental results obtained from photoemission, where the BiO-derived pockets predicted from theory, which would dope the CuO planes with additional holes, cannot yet be resolved [30].

In the face of these difficulties in the microscopic description of the BiO layers, we simulate in our model a metallic character of the BiO planes by transferring the calculated result from equation (11) as obtained for the oxygen polarizability in the (metallic) CuO plane to the oxygen

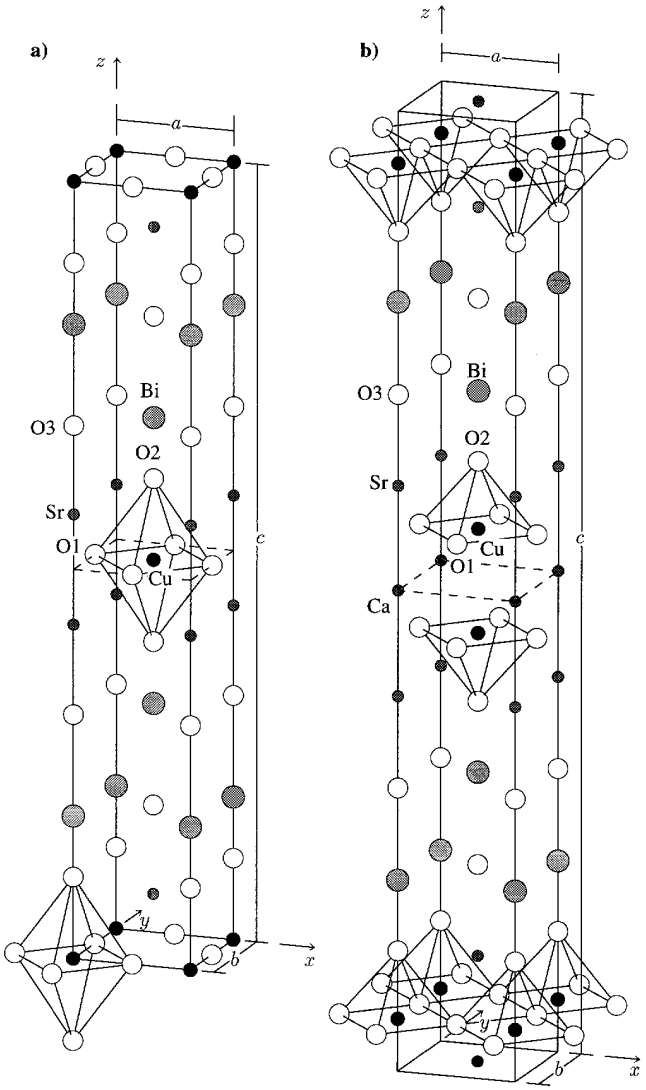

Figure 1. Elementary cells of single-layer $Bi_2Sr_2CuO_6$ (a) and bilayer $Bi_2Sr_2CaCu_2O_8$ (b) in the body-centred-tetragonal structure ($a = b$).

in the BiO layer and adjust the Bi polarizability to the same value. This choice, of course, is not unique, but the influence of a possible metallic character of the BiO layers is in principle important, also for the phonon frequencies, and should be discussed at least qualitatively. From our calculations in the following sections we find that the contributions from metallic CFs in the BiO layers lead to characteristic screening effects which leave their fingerprints in significant renormalizations of certain A_{2u} and A_{1g} modes, considerably improving agreement with the experimental data. Thus evidence is provided for the metallic character of the BiO layer. This would be consistent with BiO-derived bands crossing the Fermi surface which may lead to electron pockets as predicted by the first-principles calculations. One could also try to vary the Bi and O3 polarizabilities, which, like all the other coupling coefficients in our approach, are definite microscopic quantities with a well defined physical meaning, in order to optimize

certain phonon modes. However, this is not our concern in the present study and the choice above not only allows us to understand the qualitative effect of the metallic character of the BiO layer but additionally leads to a reasonable description of the phonon frequencies themselves. Note in this context that the various polarizabilities from equation (11) in the long-wavelength limit are a direct measure for the partial densities of states at the Fermi level [5, 6], i.e. for example of the Bi p states and the O3 p states, respectively. Thus their magnitudes express the strength of the metallic character or, in other words, the compressibility of the electrons [3] in the BiO layers.

A few words should be said about the remaining elements of the polarizability matrix from equation (11). Different families of HTSCs with different crystal structures and of different chemical compositions show in many aspects a similar behaviour. The origin of these similarities arises from the CuO layers common to all these materials. A special case is the phonon behaviour of the HTSCs where strong evidence has been provided in [4–6, 22] that the phonon anomalies, observed for the high-frequency copper–oxygen bond stretching modes [7–9], are a generic feature of the HTSC cuprates and are related to the charge fluctuations of the ions in the CuO layer. Thus, as a good approximation, the electronic structure of the CuO plane is taken as generic in our modelling and we use for the matrix elements $\Pi_{\kappa\kappa'}$ from equation (11) the results given in [5, 22] for the CuO plane in La_2CuO_4, also including off-site CFs as in [22]. Moreover, in [22] it was found that electronic bandstructures, based on the LDA, overestimate the coupling along the *c*-axis, i.e. underestimate the anisotropy of the HTSCs, and that the full matrix $\Pi_{\kappa\kappa'}$ is well approximated by its diagonal elements only. Accordingly, we allow for the CFs Cu 3d, 4s, 4p and O_{xy} 2p in the CuO plane. Consistent with this treatment we transfer the effective charges for the Cu and O_{xy} (O1) ions in the CuO plane from the tight-binding analysis of the electronic bandstructure of La_2CuO_4 ($Cu^{1.22+}$, $O1^{1.42-}$). For the apical oxygen O2 we also maintain the calculated value from the CuO octahedron in La_2CuO_4 ($O2^{1.47-}$), while the remaining effective charges for Bi-2201, i.e. Bi, Sr and O3, are determined by charge-neutrality and from the fact that the energy-minimized structure, obtained from scaling of the short-ranged part of certain pair potentials, is as close as possible to the experimental one. Note that structure optimization is important for a reliable calculation of the phonon dynamics through the dynamical matrix. For Bi-2212 we take over the values as obtained for Bi-2201 and determine the remaining effective charge for Ca from charge neutrality. Altogether, we get the following set of static effective charges: $Bi^{2.28+}$, $Sr^{1.70+}$, $Ca^{1.62+}$, $Cu^{1.22+}$, $O1^{1.42-}$, $O2^{1.47-}$ and $O3^{1.70-}$. Using these charges, we find a reasonably good solution for the energy-minimized structure for both materials. The resulting calculated values of the lattice constants *a* and *c* and the fractional atomic coordinates as well as corresponding experimental values for Bi-2201 [31] and Bi-2212 [26, 27] are shown in table 1.

The calculation of the dipole polarizability α for $Bi^{2.28+}$, $Sr^{1.70+}$, $Ca^{1.62+}$, $Cu^{1.22+}$, $O1^{1.42-}$, $O2^{1.47-}$ and $O3^{1.70-}$ is performed with the help of the modified Sternheimer method in the framework of density functional theory (DFT) in the LDA, taking self-interaction effects into account [20].

In [22] it has been found that the dipole polarizability is very anisotropic in the HTSC and dominates strongly along the (ionic) *c*-direction. So, it is a good approximation to consider dipole polarizations and corresponding DFs only in the *z*-direction parallel to the *c*-axis. In our investigation of the A_{2u} and A_{1g} modes in sections 3.2.1 and 3.2.2 we perform two types of calculation as far as the contribution of the DF is concerned. One, where the calculated *ab initio* values of the dipole polarizability α from the Sternheimer method are used for all the ions in the crystal, and a second one, where these values are scaled (reduced) in the same way as in our calculations for La_2CuO_4 [22] leading to a better agreement of the phonon dispersion with the experiments. Compared with the calculated *ab initio* values, that are normalized by

Table 1. Comparison between the experimental and calculated structures of Bi-2201 and Bi-2212. a and c are the lattice constants in Å; Z denotes the fractional atomic coordinates.

	Bi-2201		Bi-2212	
	Exp.	Calc.	Exp.	Calc.
a	3.7915	3.7962	3.814	3.8361
c	24.6182	23.9333	30.52	29.3709
Z(Bi)	0.184	0.1887	0.1978	0.2028
Z(Sr)	0.071	0.0663	0.1097	0.1040
Z(Cu)	0	0	0.0544	0.0538
Z(O1)	0	0	0.054	0.0518
Z(O2)	0.105	0.1119	0.125	0.1408
Z(O3)	0.186	0.2034	0.205	0.2140
Z(Ca)	—	—	0	0

definition to 100%, the following set of dipole polarizabilities in the z-direction has been used in the scaled version of the model: Bi (30%), Sr (30%), Ca (30%), Cu (30%), O1 (30%), O2 (100%), O3 (100%). In order to estimate the influence of the screening effects induced by the BiO layers, we study, besides the full model with CF in the CuO and BiO layers, also a dimensional restricted model, where only CFs in the CuO layer are admitted, i.e. metallic screening effects via CF are strictly confined in this case to two dimensions.

3.2. Calculated A_{2u} and A_{1g} modes in Bi-2201 and Bi-2212

According to our reasoning at the end of the last section we study in this section, besides the RIM as the corresponding reference model, the following hierarchy of models for the investigation and the discussion of the phonon modes in Bi-2201 and Bi-2212, respectively.

- SD-C: α scaled; CF only in the CuO layer.
- SD-CB: α scaled; CF in CuO and BiO layer.
- D-CB: α *ab initio*; CF in CuO and BiO layer as in model SD-CB.

A comparison of the calculated results as obtained within these three models casts light on the renormalization effect of the metallic CF and the dielectric DF, respectively, on the IR active and Raman active phonon modes. In this discussion the *ab initio* character of the RIM as the corresponding reference system is important because it allows for an unbiased discussion of these additional nonlocal screening contributions. This would not be possible in an empirical approach, because the empirical elements of a certain reference system, e.g. the fitting of the model to the phonon dispersion, may already cover the characteristic features related to the polarization of the electronic system. On the other hand, comparing the calculated values of the frequencies for the A_{2u} and A_{1g} modes obtained in the RIM with those from the microscopic models including metallic CF and dielectric DF unambiguously uncovers the specific effects from these screening contributions which are not included in the RIM. Inspection of the corresponding tables for the frequencies given below allows us to realize in detail the significance of both types of polarization process. Note in this context that in classical shell model calculations for the HTSC like those stated in this paper for the Bi-based compounds [14, 15] metallic screening has not been taken into account.

3.2.1. A_{2u} modes in Bi-2201 and Bi-2212. In table 2 we specify the frequencies of the five symmetry-allowed IR-active A_{2u} modes of Bi-2201 in the tetragonal structure calculated

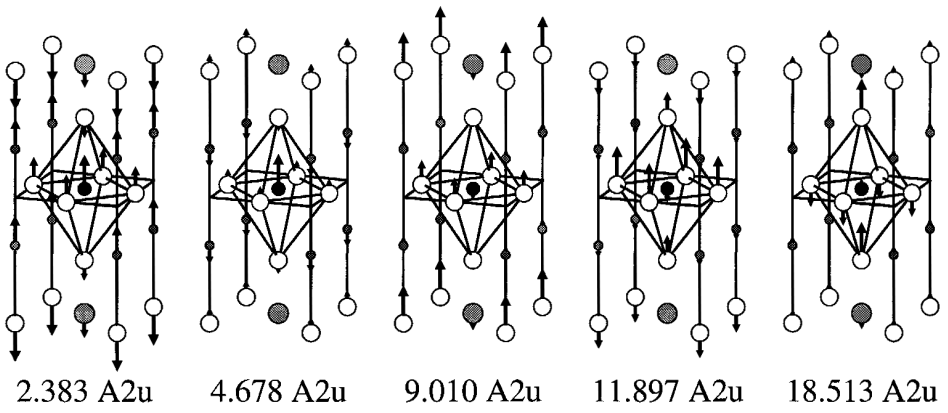

Figure 2. Displacement patterns of the five infrared-active A_{2u} symmetry modes in $Bi_2Sr_2CuO_6$ as calculated from model SD-CB. The frequency below each pattern is given in THz.

Table 2. Comparison of the calculated eigenfrequencies of the A_{2u} modes of Bi-2201 in units of cm^{-1} for different models as explained in the text with experimental results.

Bi-2201	$A_{2u}(1)$	$A_{2u}(2)$	$A_{2u}(3)$	$A_{2u}(4)$	$A_{2u}(5)$
RIM	84	164	359	590	679
SD-C	81	157	322	488	626
SD-CB	79	156	301	397	618
D-CB	75	134	258	350	560
SM [15]	77	175	293	353	596
Exp. [15]	109	165	301	385	586

from the RIM and the three microscopic models defined above. Moreover, new experimental frequencies [15] and calculated data from a classical shell model [15] are reported. Figure 2 shows the displacement patterns of the A_{2u} modes as derived from the model SD-CB. Below each pattern the calculated eigenfrequency in units of terahertz is indicated. The corresponding components of the (normalized) eigenvectors of the A_{2u} modes for model SD-CB are listed in table 3. Comparing our calculated results in table 2 with each other, we can demonstrate the influence of screening by CF and DF on the renormalization of the phonon modes. The substantial decrease in frequency for most of the modes during the transition from the RIM to the model SD-C exhibits the pure screening effect generated by the anisotropic DFs on the ions, because the CFs, allowed in this model only in the CuO layer, are forbidden by symmetry for the A_{2u} modes. A very significant renormalization in frequency arises for the $A_{2u}(4)$ mode when passing from model SD-C (488 cm^{-1}) to model SD-CB (387 cm^{-1}) which finally leads to a good agreement with the experimental value (385 cm^{-1}). The physical reason for the strong decrease in frequency is due to the metallic CFs on the ions in the BiO layers resulting in a charge transfer (CT) between the neighbouring BiO planes. This finding has been obtained from an investigation of the phonon-induced CFs in our approach. The latter are given by a calculation of the self-consistent change of the charge on an ion generated by a phonon mode $(\vec{q}\sigma)$ with frequency $\omega_\sigma(\vec{q})$ and eigenvector $\vec{e}^{\alpha}(\vec{q}\sigma)$ [3, 6]:

$$\delta\zeta_\kappa^{\vec{a}}(\vec{q}\sigma) = \left[-\sum_\alpha \vec{X}^{\kappa\alpha}(\vec{q})\vec{u}_\alpha(\vec{q}\sigma)\right] e^{i\vec{q}\cdot\vec{R}_\kappa^{\vec{a}}} \equiv \delta\zeta_\kappa(\vec{q}\sigma)e^{i\vec{q}\cdot\vec{R}^{\vec{a}}}, \tag{12}$$

Table 3. Calculated components of the eigenvectors of the A_{2u} modes of Bi-2201 and mode assignment in the SD-CB model.

Bi-2201 SD-CB	Bi(Z)	Sr(Z)	Cu(Z)	O1(Z)	O2(Z)	O3(Z)	Assignment
A_{2u}(1): 79	−0.36	0.45	0.43	0.13	−0.07	−0.23	SrCuBiO3O1
A_{2u}(2): 156	−0.01	−0.38	0.83	0.05	−0.01	0.07	CuSr
A_{2u}(3): 301	−0.25	0.05	−0.08	0.28	0.00	0.59	O3O1Bi
A_{2u}(4): 397	0.00	−0.17	−0.17	0.56	0.27	−0.27	O1O2O3SrCu
A_{2u}(5): 618	−0.16	0.04	0.07	−0.25	0.63	0.05	O2O1Bi

with the ionic displacements

$$\vec{u}_\alpha^{\vec{a}}(\vec{q}\sigma) = \left(\frac{\hbar}{2M_\alpha\omega_\sigma(\vec{q})}\right)^{1/2} \vec{e}^{\alpha}(\vec{q}\sigma)\mathrm{e}^{\mathrm{i}\vec{q}\cdot\vec{R}^{\vec{a}}} \equiv \vec{u}_\alpha(\vec{q}\sigma)\mathrm{e}^{\mathrm{i}\vec{q}\cdot\vec{R}^{\vec{a}}} \tag{13}$$

and the self-consistent reaction per unit displacement of the EDF as obtained in linear response theory from

$$\vec{X}(\vec{q}) \equiv \Pi(\vec{q})\varepsilon^{-1}(\vec{q})\vec{B}(\vec{q}) = C^{-1}(\vec{q})\vec{B}(\vec{q}). \tag{14}$$

For the Γ-point vibrations ($\vec{q} = \vec{0}, \sigma$) the following sum rule can be derived for the CF $\delta\zeta_\kappa(\Gamma\sigma)$ given by equation (12) [3]:

$$\sum_\kappa \delta\zeta_\kappa(\Gamma\sigma) = 0, \tag{15}$$

where the sum over κ denotes the CF in an elementary cell of the crystal. Physically equation (15) means that local charge-neutrality of the cell is maintained in the long-wavelength limit ($\vec{q} \to \vec{0}$) of a phonon perturbation, i.e. the phonon-induced CT is organized within the cell in such a way that from the outside the elementary cell looks neutral. Ultimately, this is a consequence of the long-ranged Coulomb interaction, resulting in screening the perturbation and minimizing thereby the increase in energy. The strong renormalization of the A_{2u}(4) mode by the induced CF in the BiO layers towards its experimental values speaks in favour of a metallic character of the BiO plane or, in the terminology of bandstructure calculations, that BiO-derived bands should dip below the Fermi level providing a possible doping mechanism for the Bi-based cuprates. The additional EDF in the form of the CF at the Bi and O3 ions in model SD-CB as compared to model SD-C admit under the restriction of equation (15) a more effective charge relaxation in response to the perturbation by the lattice displacements and to a corresponding decrease in energy of the perturbed configuration.

Now we address to the question of the reliability of the calculated *ab initio* values for the dipole polarizability α from the Sternheimer method when used for the description of screening contributions in terms of DF in the HTSC. Comparing the results for model D-CB based on the calculated *ab initio* polarizabilities with model SD-CB we find in D-CB a further increase of screening by DF and correspondingly a decrease of the frequencies. However, the agreement with the experiments is not as good as within the model SD-CB using the reduced *ab initio* dipole polarizabilities for the cations. This trend observed for the A_{2u} modes in Bi-2201 also holds true for the A_{2u} modes in Bi-2212 (table 4) and the A_{1g} modes of both materials (tables 6 and 8). So, we may conclude that the Sternheimer method most likely overestimates the dipole polarizability of the (open shell) cations while the calculated values for the oxygens O2 and O3 in the ionic layers of the HTSC seem to be described quite correctly. The reduction of the dipole polarizability for the O1 oxygen in the CuO layer in model SD-CB may be a consequence of the stronger metallic screening in the hole doped CuO plane. Altogether, the best agreement with the experiments is provided by the model SD-CB.

Table 4. Comparison of the calculated eigenfrequencies of the A_{2u} modes of Bi-2212 in units of cm^{-1} for different models as explained in the text with experimental results.

Bi-2212	$A_{2u}(1)$	$A_{2u}(2)$	$A_{2u}(3)$	$A_{2u}(4)$	$A_{2u}(5)$	$A_{2u}(6)$
RIM	79	150	285	360	595	700
SD-C	74	135	195	268	462	618
SD-CB	73	134	195	267	354	604
D-CB	60	95	142	192	344	563
SM [15]	93	195	304	343	403	643
SM [14]	137	169	277	334	487	514
FM [16]	164	225	281	442	467	617
Exp. [15]	97	168	210	304	358	583

In Bi-2212 we have six IR-active A_{2u} modes allowed by symmetry. The calculated eigenfrequencies for these modes in the RIM, SD-C, SD-CB and D-CB-models of the two-layer compound are collected in table 4, together with experimental frequencies [15], two classical shell-model calculations [14, 15] and the results from a force constant model [16]. Similarly as in Bi-2201 the frequencies of the SD-CB model are the best within our microscopic models and are in reasonably good agreement with the experiments. In the A_{2u} modes of Bi-2212, DF in the z-direction can be excited on all the ions in the crystal and, additionally to the case of Bi-2201, also CF at Cu and O1 in the CuO planes are allowed. Thus, the renormalization of the frequencies passing from the RIM to model SD-C is generated by both the DF and the CF in the CuO planes. The screening effect of the metallic CF in the BiO layers, which corresponds to the screening effect of the $A_{2u}(4)$ mode in Bi-2201, discussed above, can be seen for Bi-2212 in the $A_{2u}(5)$ mode and is most dramatic. The frequency in SD-C is 462 cm^{-1}, in SD-CB 354 cm^{-1} and in the experiment 358 cm^{-1}. In SD-C only CT between the CuO layers is induced, while in SD-BC we obtain in our calculations, additionally to the CT between the CuO layers, a strong CT between the BiO layers. Again, the additional metallic CFs at Bi and O3 lead to the correct energy relaxation and to a very good agreement with experiment. Going from model SD-CB to D-CB the most significant change in screening by increasing the dipole polarizabilities α to their *ab initio* values is seen for the $A_{2u}(4)$ mode. The agreement with the experimental results gets worse in D-CB because the calculated values of the α for the cations are too large. An analogous behaviour can be detected for the $A_{2u}(3)$ mode in Bi-2201.

The $A_{2u}(3)$ mode in Bi-2201 and the $A_{2u}(4)$ mode in Bi-2212 have an interesting displacement pattern; see figures 2 and 3 and tables 3 and 5 which we have called 'ferroelectric' in our previous calculations for La_2CuO_4 [22]. In these modes, apart from the negligible displacement of the Sr ion in $A_{2u}(3)$, all the cations vibrate coherently against the anions and as a consequence the dipole moments generated by the motion of the ions add constructively to a large value. Thus, it can be expected that these modes will have a large oscillator strength, similarly as we have found in the calculations for La_2CuO_4 [22]. Such reasoning is also consistent with the experimental results for the Bi compounds where by far the largest oscillator strength is assigned to these modes [15].

Figure 3 shows for Bi-2212 the calculated displacement patterns of the A_{2u} modes within model SD-CB and table 5 gives the corresponding components of the eigenvectors together with a detailed assignment of the modes. As already mentioned, the corresponding quantities for Bi-2201 have been represented in figure 2 and table 3, respectively.

Our results for Bi-2201 suggest that the two low-frequency modes have predominantly cation character and the three high-frequency modes oxygen character. An analogous classification also holds for the three low-frequency modes and the three high-frequency

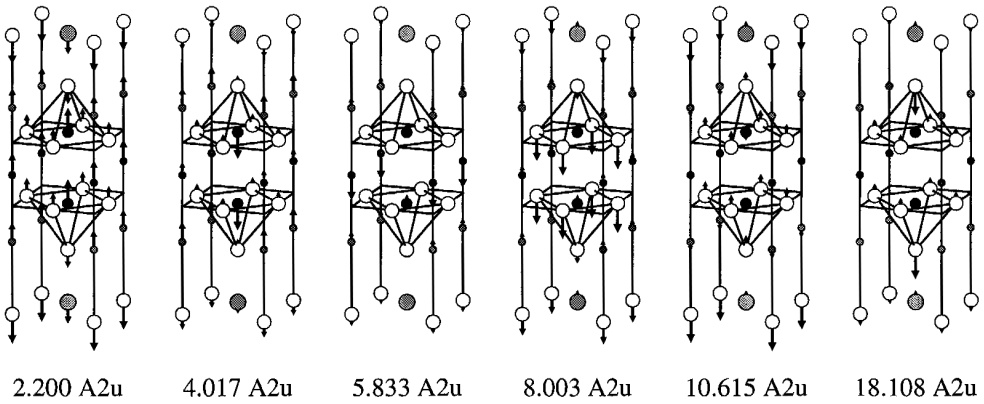

Figure 3. Displacement patterns of the six infrared-active A_{2u} symmetry modes in $Bi_2Sr_2CaCu_2O_8$ as calculated from model SD-CB. The frequency below each pattern is given in THz.

Table 5. Calculated components of the eigenvectors of the A_{2u} modes of Bi-2212 and mode assignment in SD-CB model.

Bi-2212 SD-CB	Bi(Z)	Sr(Z)	Ca(Z)	Cu(Z)	O1(Z)	O2(Z)	O3(Z)	Assignment
$A_{2u}(1)$: 73	−0.42	0.31	0.26	0.36	0.09	−0.09	−0.21	BiCuSrCaO3
$A_{2u}(2)$: 134	−0.04	0.45	0.13	−0.53	0.04	0.01	−0.07	CuSrCa
$A_{2u}(3)$: 195	0.00	0.23	−0.93	0.10	0.01	0.00	−0.06	CaSrCu
$A_{2u}(4)$: 267	0.17	0.13	0.10	0.09	−0.43	−0.07	−0.27	O1O3BiSrCa
$A_{2u}(5)$: 354	0.17	−0.17	−0.01	−0.05	0.18	0.15	−0.60	O3O1BiSrO2
$A_{2u}(6)$: 604	0.17	−0.02	−0.01	−0.02	0.10	−0.67	−0.05	O2BiO1

modes in Bi-2212. Our mode assignment for the A_{2u} modes in both materials qualitatively is in agreement with that obtained from the shell model [15] which has been used for the interpretation of the new experimental results in the same work.

According to table 3 and figure 2 in the lowest-frequency mode, $A_{2u}(1)$, the motion of Bi is strongly mixed with out-of-phase motion of Sr and Cu and with a smaller contribution of O3 and O1 motion. In the next mode, $A_{2u}(2)$, Cu vibrates against Sr. In the ferroelectric mode, $A_{2u}(3)$, the cations, apart from the small Sr amplitude, vibrate against the oxygens O3 and O1. In $A_{2u}(4)$ predominantly O1 and to a smaller extent O2 vibrate against O3, while the highest-frequency mode clearly has O2 apical character.

From table 5 and figure 3 we see that the Bi-2212 lowest-frequency mode, $A_{2u}(1)$, is characterized by a vibration of Cu, Sr and Ca against Bi. A smaller oxygen contribution from different layers is also present. The next mode, $A_{2u}(2)$, is mostly due to the motion of Cu against Sr with a small contribution from Ca. In the $A_{2u}(3)$ mode Ca vibrates against Sr and Cu. $A_{2u}(4)$ is the ferroelectric mode for the two-layer material, where the oxygen ions, essentially O1 and O3, vibrate against the cations. In $A_{2u}(5)$ predominantly O3 vibrates against O1 and O2. There are in addition some smaller contributions from Bi and Sr. Finally, the mode with the highest frequency is, similarly as in Bi-2201, predominantly an apical oxygen (O2) mode.

Obviously, because of the bilayer coupling, there is a significant change in the character of the modes with the second highest frequency in the two materials from O1:O3 in Bi-2201 ($A_{2u}(4)$) to essentially O3 with only a small O1 component left in Bi-2212 ($A_{2u}(5)$). This change in mode behaviour is also accompanied by a charge transfer between the

Table 6. Comparison of the calculated eigenfrequencies of the A_{1g} modes of Bi-2201 in units of cm^{-1} for different models as explained in the text with experimental results.

B-2201	$A_{1g}(1)$	$A_{1g}(2)$	$A_{1g}(3)$	$A_{1g}(4)$
RIM	142	230	484	724
SD-C	128	209	384	659
SD-CB	120	166	378	595
D-CB	116	163	271	576
SM [15]	111	229	423	575
Exp. [32]	120	200	459	625

CuO planes in the bilayer compound, a screening effect, which is not possible in Bi-2201. Correspondingly, from the different mode behaviour we expect a characteristic change in the oscillator strengths for these modes in the different materials which indeed has been observed in the experiments [15].

3.2.2. A_{1g} modes in Bi-2201 and Bi-2212. Due to the reduction of symmetry, e.g. by the structural modulation of the BiO layers, a larger number of Raman-active phonon modes occur in the experimental spectra of the Bi-based cuprates than would be allowed by the idealized body-centred-tetragonal structure [17, 32].

From the latter symmetry we expect four A_{1g} modes for Bi-2201 and six A_{1g} modes in Bi-2212, which are symmetric *c*-axis vibrations. While the frequencies measured by different groups agree quite well, the phonon assignment is contradictory and has changed during the last few years. In the following we report our predictions of the frequencies, the displacement patterns and the components of the eigenvectors of the A_{1g} modes in Bi-2201 and Bi-2212.

In the case of Bi-2201 for the A_{1g} modes CFs are allowed by symmetry on all the ions in the CuO and BiO layers. Note that CFs in the CuO layer are forbidden for the A_{2u} modes for symmetry reasons. DFs in the z-direction can be excited at Bi, Sr, O2 and O3 but not in the CuO planes which, on the other hand, is possible for A_{2u}. Table 6 collects our calculated results, data from a shell model [15] and experimental values [32].

Passing from the RIM to model SD-C the renormalization effect of the frequencies can be attributed to both CF as well as DF. The softening of the frequencies going from SD-C to SD-CB is physically related to the CT from the BiO layers to the CuO layer and vice versa. This effect is predominantly visible for the $A_{1g}(2)$ and $A_{1g}(4)$ modes. Finally, as is also the case with the A_{2u} modes, using the *ab initio* data for the dipole polarizability for the cations in model D-CB leads to a further decrease of the frequencies, which is particularly large for $A_{1g}(3)$.

Altogether, with the model SD-CB, where additionally metallic CFs are allowed in the BiO layers, a reasonably good agreement with the experiments is achieved. According to figure 4 and table 7 we can predict the following mode assignment. In the lowest-frequency mode, $A_{1g}(1)$, we have an in-phase motion of Bi, Sr and the apical oxygen O2. In the next mode, $A_{1g}(2)$, predominantly Sr vibrates against Bi and O3. $A_{1g}(3)$ is almost exclusively an O3 vibration, while the mode with the highest frequency is the O2 apical oxygen mode. Comparing our assignment with the experiments [32], we find an agreement for the two low-frequency modes but not for the two high-frequency modes where a reversed assignment is reported ($A_{1g}(3) - 460 : O2$; $A_{1g}(4) - 630 : O3$). However, these modes also appear in the Raman spectra of Bi-2212 [17, 18] and there is a strong dispute concerning the origin of the two highest frequencies around 460 and 630 cm^{-1}. Most authors have assigned the 460 cm^{-1} mode to O2 vibrations and the 630 cm^{-1} mode to O3. Recently, however, arguments have

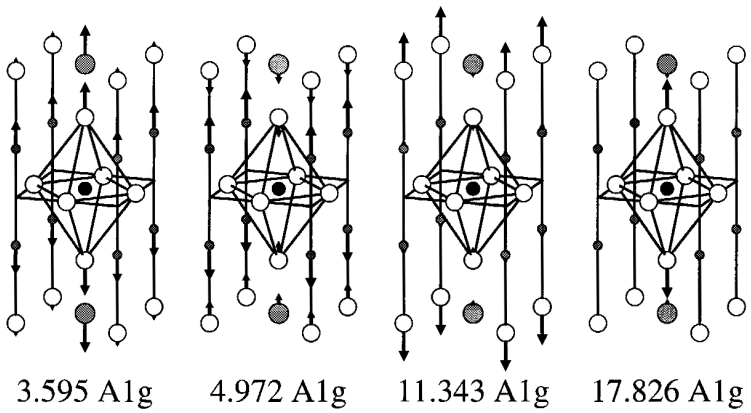

Figure 4. Displacement patterns of the four Raman-active A_{1g} symmetry modes in $Bi_2Sr_2CuO_6$ as calculated from model SD-CB. The frequency below each pattern is given in THz.

Table 7. Calculated components of the eigenvectors of the A_{1g} modes in Bi-2201 and mode assignment in the SD-CB model.

Bi-2201 SD-CB	Bi(Z)	Sr(Z)	O2(Z)	O3(Z)	Assignment
$A_{1g}(1)$: 120	0.62	0.31	0.15	0.01	BiSrO2
$A_{1g}(2)$: 166	−0.29	0.63	−0.08	−0.12	SrBiO3
$A_{1g}(3)$: 378	−0.06	0.10	−0.02	0.70	O3Sr
$A_{1g}(4)$: 595	−0.17	0.01	0.69	0.01	O2Bi

been presented that the assignment should be reversed [17, 18]. This would be consistent with our theoretical prediction for the assignment of these modes in Bi-2201 as well as in Bi-2212, see below.

In Bi-2212, additionally to the CF and DF allowed by symmetry in Bi-2201, DF in the z-direction can be excited in the CuO layers. In table 8 we have listed our calculated results, the data from two classical shell model calculations [14, 15] and from a force constant model [16]. In the last row of the table experimental results from [17] are given. As for Bi-2201 the softening of the frequencies from RIM to SD-C is due to CF and DF and that from SD-C to SD-CB from the additional CF in the BiO layers. Remarkable is the softening for $A_{1g}(5)$ and $A_{1g}(6)$ which is generated by the CT between the CuO and BiO layers. Partly, a strong decrease of the frequencies is found if the *ab initio* values for the dipole polarizability are used for the cations in model D-CB. As is also the case for the other phonon models discussed in this work the overall agreement with the experiments is best for the model SD-CB.

Figure 5 and table 9 contain our predictions of the mode assignment of the A_{1g} modes in Bi-2212. The lowest-frequency $A_{1g}(1)$ mode involves the in-phase motion of the Sr, Bi and Cu ions. In $A_{1g}(2)$ essentially Bi is out of phase with Cu and in $A_{1g}(3)$ Sr vibrates against Cu and Bi. Oxygen vibrations are only weakly excited in these three low-frequency modes.

On the other hand, the three high-frequency modes are predominantly oxygen modes. $A_{1g}(4)$ is an in-phase O3:O1 mode, in $A_{1g}(5)$ O3 is out of phase with O1 and O2, while the highest-frequency mode is essentially an apical oxygen O2 mode, which is consistent with recent experimental work [17, 18].

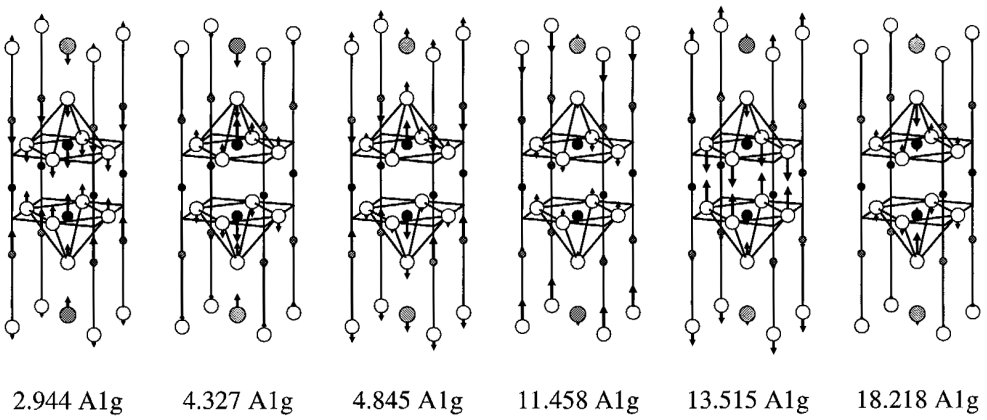

Figure 5. Displacement patterns of the six Raman A_{1g} symmetry modes in $Bi_2Sr_2CaCu_2O_8$ as calculated from model SD-CB. The frequency below each pattern is given in THz.

Table 8. Comparison of the calculated eigenfrequencies of the A_{1g} modes of Bi-2212 in units of cm^{-1} for different models as explained in the text with experimental results.

Bi-2212	$A_{1g}(1)$	$A_{1g}(2)$	$A_{1g}(3)$	$A_{1g}(4)$	$A_{1g}(5)$	$A_{1g}(6)$
RIM	125	157	196	493	598	730
SD-C	115	147	178	399	508	656
SD-CB	98	144	162	382	451	608
D-CB	94	132	151	269	359	570
SM [15]	112	149	208	370	461	630
SM [14]	87	164	182	387	494	517
FM [16]	80	123	170	316	459	616
Exp. [17]	59	117	145	409	463	627

Table 9. Calculated components of the eigenvectors of the A_{1g} modes of Bi-2212 and mode assignment in the SD-CB model.

Bi-2212 SD-CB	Bi(Z)	Sr(Z)	Cu(Z)	O1(Z)	O2(Z)	O3(Z)	Assignment
$A_{1g}(1)$: 98	−0.35	−0.48	−0.34	−0.09	−0.09	0.03	SrBiCu
$A_{1g}(2)$: 144	−0.51	0.03	0.46	0.07	−0.13	−0.04	BiCuO2
$A_{1g}(3)$: 162	0.29	−0.50	0.38	0.02	0.08	0.07	SrCuBi
$A_{1g}(4)$: 382	0.06	−0.05	0.05	−0.16	−0.04	−0.66	O3O1
$A_{1g}(5)$: 451	0.05	0.10	0.13	−0.43	−0.21	0.23	O1O3O2CuSr
$A_{1g}(6)$: 608	0.16	−0.03	−0.04	0.15	−0.65	−0.03	O2BiO1

4. Summary and conclusions

Based on an *ab initio* RIM as an unbiased reference system, we have calculated, within a linear response approach, the *c*-axis lattice dynamics of the Bi-based cuprate superconductors Bi-2201 and Bi-2212 taking into account CF and anisotropic DF as nonlocal electronic polarization processes.

We have performed detailed calculations of the frequencies for the infrared-active A_{2u} modes and the A_{1g} Raman modes and have studied the interplay of screening by CF and DF with the renormalization of these modes. Our calculated results for the infrared-active A_{2u}

modes are in good agreement with new experiments on single crystals. A reasonably good agreement with experiment is also obtained for the A_{1g} Raman modes. The experimentally as well as theoretically interesting question of a possible metallic character of the BiO layers has been discussed in the light of typical and very strong renormalization effects of certain A_{2u} and A_{1g} modes by metallic CF in the BiO layers. From the comparison of the calculated frequencies with the corresponding experimental ones evidence of the metallic behaviour of the BiO layers has been provided. This speaks in favour of the opinion that the BiO planes play the role of an electron attracting reservoir and therefore may dope the CuO layers with holes. In context with a metallic character of the BiO layers and its influence on the phonons the effect of the structural modulation of the BiO planes remains an open and very complex question.

We have then presented calculations for the displacement patterns and the components of the (normalized) eigenvectors of the A_{2u} and A_{1g} modes in Bi-2201 and Bi-2212. From these calculations corresponding mode assignments have been proposed. This may help to clarify the rather controversially discussed assignments in the experimental literature for the infrared and the Raman phonons in the Bi-based compounds. As far as the heavy dispute about the origin of the two highest Raman frequencies is concentrated, our calculations clearly predict the O2 apical oxygen mode as the one with the highest frequency which is consistent with recent experiments. In the case of the A_{2u} modes likewise the apical oxygen mode is predicted by our calculations to have the highest frequency. A conspicuous change in the behaviour of the A_{2u} modes with the second highest frequency in Bi-2001 and Bi-2212, respectively, related to the bilayer coupling, has been found in our calculations, and the corresponding change in the optical conductivity spectra has been observed experimentally. Finally, we detect in both Bi-compounds ferroelectric-like modes which are expected to contribute significantly to the low-frequency optical response. Such a mode was previously also seen in La_2CuO_4, dominating the infrared response along the *c*-axis in this material.

Acknowledgments

We are grateful to N Kovaleva for sending the manuscript [15] prior to publication. Financial support by the Deutsche Forschungsgemeinschaft is greatly appreciated.

References

[1] Allen P B 1977 *Phys. Rev.* B **16** 5139
[2] Lanzara A, Bogdanov P V, Zhou X J, Kellar S A, Feng D L, Lu E D, Yoshida T, Eisaki H, Fujimori A, Kishio K, Shimoyama J I, Noda T, Uchida S, Hussain Z and Shen Z X 2001 *Nature* **412** 510
[3] Falter C, Klenner M and Ludwig W 1993 *Phys. Rev.* B **47** 5390
[4] Falter C, Klenner M, Hoffmann G A and Chen Q 1997 *Phys. Rev.* B **55** 3308
[5] Falter C and Hoffmann G A 2000 *Phys. Rev.* B **61** 14537
[6] Falter C and Hoffmann G A 2001 *Phys. Rev.* B **64** 054516
[7] Pintschovius L and Reichardt W 1998 *Neutron Scattering in Layered Copper-Oxide Superconductors Physics and Chemistry of Materials with Low Dimensional Structures* vol 20, ed A Furrer (Dordrecht: Kluwer)
[8] McQueeney R J, Petrov Y, Egami T, Yethiray M, Shirane G and Endoh Y 1999 *Phys. Rev. Lett.* **82** 628
[9] Pintschovius L and Braden M 1999 *Phys. Rev.* B **60** R15039
[10] Falter C and Hoffmann G A 1998 *Phys. Rev.* B **57** 14444
[11] Falter C, Hoffmann G A and Schnetgöke F 2002 *J. Phys.: Condens. Matter* **14** 3239
[12] Tajima S, Gu G D, Miyamoto S, Odagawa A and Koshizuka N 1993 *Phys. Rev.* B **48** 16164
[13] Tsvetkov A A, Dulic D, van der Marel D, Damascelli A, Kaljushnaia G A, Gorina J I, Senturina N N, Kolesnikov N N, Ren Z F, Wang J H, Menovsky A A and Palstra T T M 1999 *Phys. Rev.* B **60** 13196
[14] Prade J, Kulkarni A D, de Wette F W, Schröder U and Kress W 1989 *Phys. Rev.* B **39** 2771

[15] Kovaleva N *et al* 2003 arxiv: cond-mat/0307509
[16] Chun S J and Wu S Z 1991 *Phys. Status Solidi* b **163** K49
[17] Kakihana M, Osada M, Käll M, Börjesson L, Mazaki H, Yasuoka H, Yashima M and Yoshimura M 1996 *Phys. Rev.* B **53** 11796
[18] Pantoja A E, Pooke D M, Trodahl H J and Irwin J C 1998 *Phys. Rev.* B **58** 5219
[19] Williams G V M, Pooke D M, Pringle D J, Trodahl H J, Tallon J L, Quilty J, Malde N, Macmanus-Driscoll J L, Crossley A and Cohen L F 2000 *Phys. Rev.* B **62** 1379
[20] Falter C, Klenner M, Hoffmann G A and Schnetgöke F 1999 *Phys. Rev.* B **60** 12051
[21] Falter C, Klenner M and Hoffmann G A 1995 *Phys. Rev.* B **52** 3702
[22] Falter C and Schnetgöke F 2002 *Phys. Rev.* B **65** 054510
[23] Krakauer H, Pickett W E and Cohen R E 1998 *J. Supercond.* **1** 111
[24] Etrillard J, Bourges P and Lin C T 2000 *Phys. Rev.* B **62** 150
[25] Jakubowicz N, Grebille D, Hervieu M and Leligny H 2001 *Phys. Rev.* B **63** 214511
[26] Tarascon J M, Le Page Y, Barboux P, Bagley B G, Greene L H, McKinnon W R, Hull G W, Giroud M and Hwang D M 1988 *Phys. Rev.* B **37** 9382
[27] Tarascon J M, McKinnon W R, Barboux P, Hwang D M, Bagley B G, Greene L H, Hull G W, Le Page Y, Stoffel N and Giroud M 1988 *Phys. Rev.* B **38** 8885
[28] Pickett W E 1989 *Rev. Mod. Phys.* **61** 433
[29] Singh D J and Pickett W E 1995 *Phys. Rev.* B **51** 3128
[30] Damascelli A, Hussain Z and Shen Z X 2003 *Rev. Mod. Phys.* **75** 473
[31] Torardi C C, Subramanian M A, Calabrese J C, Gopalakrishnan J, McCarron E M, Morrissey K J, Askew T R, Flippen R B, Chowdhry U and Sleight A W 1988 *Phys. Rev.* B **38** 225
[32] Lin R, Klein M V, Han P D and Payne D A 1992 *Phys. Rev.* B **45** 7392